SPATIAL AND TEMPORAL PATTERNS OF GLOBAL H5N1 OUTBREAKS

Y.L. Si [a,c,] *, P. Debba [b], A. K. Skidmore [a], A. G. Toxopeus [a], L. Li [c]

[a] ITC, Department of Natural Resources, 7500AA Enschede, The Netherlands – (yali, skidmore, toxopeus)@itc.nl
[b] Council for Scientific and Industrial Research (CSIR), Logistics and Quantitative Methods, CSIR Built Environment, P. O. Box 395, 0001, South Africa - pdebba@csir.co.za
[c] School of Resources and Environmental Science, Wuhan University, Luoyu Road 129, 430079 Wuhan, China - lilin@whu.edu.cn

Commission II, WgS II/1

KEY WORDS: H5N1, GIS, Spatial, Temporal, Global, Hot spots

ABSTRACT:

The global spread of highly pathogenic avian influenza (H5N1) in wild birds and poultry is considered a significant pandemic threat. Furthermore, human infections resulting from direct contact with infected birds/poultry pose a serious public health threat. From November 2003 to March 2007, a total of 3345 H5N1 outbreaks were reported worldwide. Spatial and temporal patterns can provide clues in understanding the dynamics of disease spread. However, little has been done to explore these patterns of H5N1 outbreaks during this period at the global scale. The objective of this research is to detect spatial, temporal and space-time clustering using geostatistical methods. Data from histological confirmed cases of H5N1were obtained from a Dutch web site and a Google earth data. Kernel estimation, *G* and *F* functions were used to test the first-order and the second-order spatial clustering respectively. An autocorrelation function and a periodogram were used to detect the temporal clustering. In addition, Knox's test, space-time K-function and space-time scan statistics were used to explore the space-time clustering. The Monte Carlo simulation was used to test the significance of the clustering. Examination of spatial and temporal patterns indicates significant spatial clustering and seasonal cyclicity. The Monte Carlo test revealed strong evidence for space-time clustering of H5N1 cases and the location of significant space-time clusters were detected. The results are considered to be valuable for global H5N1 surveillance, prevention and possible future outbreaks controlling.

1. INTRODUCTION

H5N1 Avian influenza, commonly called "bird flu", is an infectious disease of birds caused by strains of the influenza virus. The first H5N1 virus was isolated from a farmed goose in southern China in 1996 (WHO 2007). Following this, the first case of avian influenza viruses in humans occurred in Hong Kong (China) in 1997 (WHO 2007). The present outbreak of the H5N1 virus began in December 2003, when South Korea identified the virus in poultry populations (WHO 2004). From December 2003 to February 2007, a total of 3345 H5N1 outbreaks in birds and poultry were reported worldwide and 277 people were infected, 167 died (OIE 2006). The global spread of highly pathogenic avian influenza (H5N1) in wild birds and poultry is considered a significant pandemic threat. Furthermore, human infections resulting from a direct contact with these infected birds/poultry pose a serious public health threat.

Spatial and temporal patterns can provide clues in understanding the dynamics of disease spread. Detection of spatial, temporal and space-time clustering is useful in identifying higher risk areas and times, where disease surveillance and control should be targeted. Several methods are proposed for spatial and temporal patterns analysis. Kernel estimation and nearest neighbour analysis are selected in this research because they are widely used in exploring spatial point processes at first order and second order (Gatrell et al. 1996, Walter et al. 2005). The autocorrelation function and periodogram are used for temporal pattern analysis, to detect the seasonality of the disease outbreak (Diggle 1990, French et al. 1999). For space-time interactive analysis, Knox's test is a popular and simple method that has been extensively used by others (Kulldorff and Hjalmars 1999, Norstrom et al. 2000, Rogerson 2001). Space-time K function is another valuable method for exploring the space-time clustering because of the advantages of incorporating multiple cut-offs and the graphical visualizations (French et al. 2005, McNally et al. 2006, Wilesmith et al. 2003). Spatial scan statistics localize the specific space-time clusters, which can be used for hot spot area identification (Kulldorff 1997, Kulldorff et al. 2005).

The spatial and temporal patterns of H5N1 at a local level within a short period have been explored in some areas, like Southern China (Oyana et al. 2006), Italy (H7N1) (Mulatti et al. 2007) and Romania (Ward et al. 2008). However, no research has been done to explore these patterns of the H5N1 at the global scale within a 3-year period. The objective of this research is to explore the spatial and temporal patterns of highly pathogenic H5N1 at global level. The hypotheses of this research are (1) the outbreak of H5N1 showed clustering in geographical space; (2) the outbreak of H5N1 has the character of seasonal cycle in temporal pattern; (3) significant space-time clustering occurred under specific spatial and temporal cut-offs;

* Corresponding author

(4) the location of space-time clusters showed the hot spots of H5N1 outbreaks.

2. METHODS AND MATERIALS

2.1 Data

A Google earth data layer named "time series of H5N1 outbreaks" was obtained for this research as the main data source. The data layer was organized by Declan Butle based on historical confirmed cases of H5N1. These reports can be found at the following internet web site (http://www.oie.int/downld/AVIAN%20INFLUENZA/A_AI-Asia.htm) and a Dutch web site (http://vogelgriep.startpagina.nl/). For spatial and temporal pattern analysis, the data was converted to a geospatial point data format (ESRI shapefile). The time and geographical location of all reported outbreaks of H5N1 from December 2003 to March 2007 were stored in the attribute table of an ESRI shapefile. The point map was placed in an equidistant cylindrical projection. For pure temporal pattern analysis, the time range of the data is from December 2003 to December 2007.

2.2 Spatial Clustering Analysis

Spatial stochastic processes may be characterized in terms of first-order and second-order properties (Bailey and Gatrell 1995). The first-order properties are described in terms of the intensity of the process, which is the mean number of events per unit area of the points in a region *R*. The second-order properties involve the relationship between the number of events in pairs of sub-region within *R*. In this study, kernel estimation was used to detect the first-order properties of the disease outbreak patterns and the *G* and *F* functions were used to detect the second-order properties of the disease outbreak patterns.

Kernel estimation is used to obtain a smooth estimate of a univariate or multivariate probability density from an observed sample of observations. If *s* represents a general location in *R* and s_1, ..., s_n are the locations of the *n* observed events then the intensity, $\lambda(s)$, at *s* is estimated by

$$\hat{\lambda}_\tau(s) = \frac{1}{\delta_\tau(s)} \sum_{i=1}^{n} \frac{1}{\tau^2} k\left(\frac{s - s_i}{\tau}\right) \qquad (1)$$

where *k* () is the kernel weighting function which is symmetric about the origin and $\delta_\tau(s)$ is used for the edge-correction. The kernel weighting function is centered on *s* and "stretched" according to the parameter $\tau > 0$, which is referred to as the bandwidth.

The *G* and *F* functions are designed to investigate second order properties using distances between observed events in the study area (Bailey and Gatrell 1995). The *G* function estimates the empirical cumulative probability of the distance from a random event to the nearest other event below or equal to *h*. The *F* function estimates the probability of the distance from a random location to the nearest event. Both *G* and *F* functions are based on nearest neighbour test. However, they have a distinct difference. The *G* function describes the spatial distribution mode by inter-event attraction. If it climbs very steeply in the early part of its range before flattening out, then this would imply clustering. The *F* function describes the distribution mode by random point-event dispersion. If the *F* function climbs very slowly in the early part of its range, then this would imply clustering. The significance of the clustering was detected by comparing the estimated distribution functions with a simulation estimate of their theoretical distribution functions under complete spatial randomness (CSR). Ninety-nine simulations were generated to make the significant level equal to 0.01. These statistical analyses were executed using the **R** statistical software and the **R** packages *splancs* and *maptools*.

2.3 Temporal Clustering Analysis

The temporal pattern was explored by estimating the autocorrelation function and the periodogram (Diggle 1990). The autocorrelation function describes the correlation between the processes at different points in time. Here we summarized the relationship between the cases in each month and the cases in previous months for a defined time lag (*k*). The autocorrelation function value ranges from -1 to 1. High positive values indicate strong positive association while large negative values indicate strong negative association. The high degree of correlation at a time lag of k_i means there is a strong cyclical pattern within k_i months. In the case of cyclic patterns in the data, the data is usually detrended by fitting a least squares regression line and then each value is subtracted from the fitted values using the estimated regression equation. The autocorrelation function was calculated for the residuals of the fitted model and the lags ranged from 0 to a maximum of 48 months.

The periodogram is a summary description based on a representation of an observed time series as a superposition of sinusoidal waves of different frequencies. The data is fitted to sinusoidal waves with Fourier frequencies using least squares methods (Diggle 1990). Each periodogram ordinate, which is proportional to the amplitude of the fitted sinusoidal wave and its variance, was plotted against the given Fourier frequency to show the contribution of cyclical components to the temporal pattern. The statistical software R and a contributed package *pgam* were used to calculate the autocorrelation function and periodogram respectively.

2.4 Space-Time Clustering Analysis

Space-time clustering occurs when excess numbers of cases of a disease are observed within small geographical locations at limited periods of time and this cannot be explained in terms of general excesses in those locations or at those times.

Knox's test is a simple space-time interaction test, which uses as the test statistic the number of pairs of events that are within defined critical time and space values (Knox and Bartlett 1964). Each individual pair is compared in terms of distance and time interval defined by the user. A 2×2 contingency table is formed by classifying the $n(n-1)/2$ pairs of cases as close in space and time, close in space only, close in time only, or close in neither space nor time. The expected number is obtained by the cross-products of the columns and row totals. The different between the observed number of pairs in each cell and the expected number is measured with a Chi-square statistic. According to the previous research (Picado et al. 2007, Wilesmith et al. 2003) and the mean distance and time intervals, two critical spatial distances (10 and 4374 km) and two temporal distances (21 and 320 days) were selected to do the

Knox test. One thousand Monte Carlo simulations of the chi-square value under spatial randomness were calculated to test the significance of the space-time clustering. Knox test was carried out using software CrimeStat III (version 3.1 http://www.icpsr.umich.edu/CRIMESTAT/).

Space-time *K* function provides informal graphical methods to describe the space-time clustering at different scales. It defines the expected number of events within a distance *d* and time interval *t* of an arbitrary event, scaled by the expected number of events per unit area and per unit time. An appropriate edge-corrected estimate of $K(d,t)$ derived from *K* function is therefore

$$\hat{K}(d,t) = \frac{RT}{n^2} \sum_{i \neq j} \sum \frac{I_d(d_{ij}) I_t(t_{ij})}{w_{ij} v_{ij}} \qquad (2)$$

where *R* is the area of the region, T is the overall time span observed, n is the observed number of events, d_{ij} is the distance between the i th and the j th observed events, $I_d(d_{ij})$ is an indicator function that takes the value 1 when d_{ij} is less than d and 0 otherwise, t_{ij} is the time interval between the i th and the j th observed events, $I_t(t_{ij})$ is an indicator function which is 1 if $t_{ij} \leq t$ and 0 otherwise, w_{ij} is the conditional probability that an event is observed in R, given that it is a distance d_{ij} from the i th event, and v_{ij} is the temporal equivalent of the spatial-edge correction based upon whether a time interval centered on *i* of length t_{ij} lies wholly within the $(0,T)$ time span observed (Diggle et al. 1995).

If there is an absence of space-time interaction, K_{dt} should be the product of separate space $K_D(d)$ and time $K_T(t)$ function. Thus the function of exploring space-time interaction is

$$\hat{D}(d,t) = \hat{K}(d,t) - \hat{K}_D(d)\hat{K}_T(t) \qquad (3)$$

Peaks on the surface of $\hat{D}(d,t)$ indicate space-time interaction when plotted against space and time. To facilitate comparison among time periods, a relative measure of $D_0(s,t)$ was calculated to represent the excess risk attributable to the space-time interaction (Diggle et al. 1995).

$$\hat{D}_O(d,t) = \frac{\hat{D}(d,t)}{\hat{K}_D(d)\hat{K}_T(t)} \qquad (4)$$

To avoid first-order effects, a small maximum distance of 10 km and a maximum time separation of 21 days were selected in accordance with previous researches (Picado et al. 2007, Wilesmith et al. 2003). To test the significance of the space-time interactive, 999 Monte Carlo simulations were calculated by randomly permuting the time labels to the fixed spatial locations. The sum of $\hat{D}(d,t)$ over 999 *d* and *t* were obtained. The sum of $\hat{D}(d,t)$ for the observed data was ranked among the empirical frequency of nine hundred and ninety nine sums. The significant level was determined by the rank of the observed data. These analyses were carried out using R software and the contributed packages *spatstat*, *splancs* and *maptools*.

Space-time *K* function was used to test whether space-time clustering occurs throughout the map, according to both small clusters of slightly larger than average incidence rate and weakly interacting events (Assuncao et al. 2007). However, to detect and localize the specific space-time clusters is also very important for disease control and surveillance. The spatial scan statistic has been developed to test for geographical clusters and to identify their approximate location (Kulldorff 1997). The space-time permutation model was selected because it does not need population at risk data and only requires the number of cases in each area for each time period (Kulldorff 2006).

The space-time permutation scan statistic utilizes many overlapping cylinders to define the scanning window. After iterating over a finite number of geographical grid points (if no grid file is specified, the coordinates are used as the centroids of the circles), the circle radius is increased from zero to a maximum spatial searching radius. The height of the cylinder represents the number of days. The last day is always included together with some preceding days, up to a maximum temporal range. Initially the total number of observed cases (*C*) was calculated, where z is some defined area and d is some specific day:

$$C = \sum_z \sum_d c_{zd} \qquad (5)$$

Then, for each area and day, the expected number of cases μ_{zd} was calculated conditioning on the observed marginal and is given by

$$\mu_{zd} = \frac{1}{C}\left(\sum_z c_{zd}\right)\left(\sum_d c_{zd}\right) \qquad (6)$$

The expected number of cases μ_A in a specific cylinder *A* is the summation of all expected cases within that cylinder. Hence μ_A is defined as

$$\mu_A = \sum_{(z,d) \in A} \mu_{zd} \qquad (7)$$

Let c_A be the observed number of cases in the cylinder, when both $\sum_{z \in A} c_{zd}$ and $\sum_{d \in A} c_{zd}$ are small compared to *c*, then c_A is approximately Poisson distributed. The Poisson generalized likelihood ratio was calculated as a measure of containing an outbreak in cylinder A and is given by

$$\left(\frac{c_A}{\mu_A}\right)^{c_A}\left(\frac{c-c_A}{c-\mu_A}\right)^{c-c_A} \qquad (8)$$

Among all the cylinders evaluated, the one with the maximum generalized likelihood ratio is most likely to constitute the space-time cluster, and to include a true outbreak (Kulldorff et al. 2005). Monte Carlo test was used to evaluate the statistical significance of the clustering.

The space-time permutation model was executed based on outbreak data instead of cases because of the inadequate case information. The maximum spatial and temporal window cannot exceed 50% of the population at risk and 50% of study

period (Kulldorff 2006). In order to allow both small and large clusters to be detected, and according to the result of parameter sensitive analysis, the maximum spatial and temporal scanning window size was defined as 40 km and 40 days to get maximum number of clusters. 999 Monte Carlo simulations were executed to allow the smallest *p*-value to be 0.001. These analyses were carried out using the software SaTScan (http://www.satscan.org).

3. RESULTS

3.1 Spatial Clustering Analysis

3.1.1 Kernel Estimation: The distribution of the H5N1 outbreaks in poultry and birds from December 2003 to February 2007 is shown in figure 1(a). The shallow point shows the specific location of each outbreak. Kernel density was calculated to show the first-order spatial property of the H5N1 outbreaks. The kernel density is displayed in figure 1(b). Darker regions denote higher outbreak density. Most of the outbreaks are distributed in South Asia, East Russia, West Europe, Black Sea, and East Africa, with the highest outbreak density in South Asia.

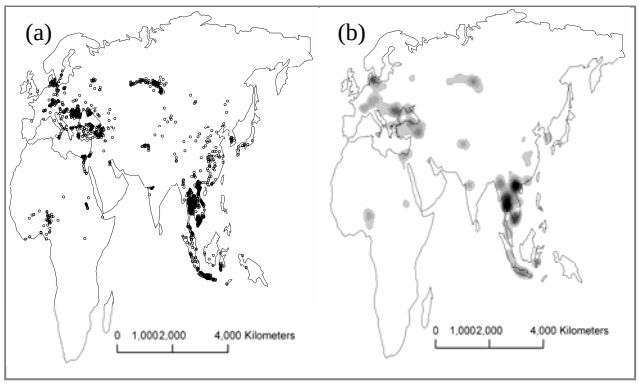

Figure. 1. (a) The spatial distribution of 3345 histological confirmed H5N1 outbreaks in poultry and birds from December 2003 to February 2007 worldwide; (b) Kernel estimation of H5N1 outbreaks.

3.1.2 *G* and *F* Function: The estimated *G* function line is located above the upper envelope of simulated *G* under CSR (figure 2(a)), and the estimated *F* function is located below the lower envelope of simulated *F* under CSR (figure 2(b)), which suggest significant spatial clustering $(p = 0.01)$.

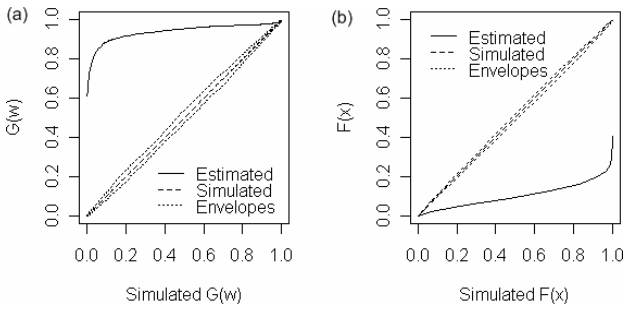

Figure. 2. (a) Estimated *G* (*w*) against simulated *G* (*w*) with upper and lower envelopes under complete spatial randomness (*p*-value = 0.01); (b) Estimated *F* (*x*) against simulated *F* (*x*) with upper and lower envelopes under complete spatial randomness (*p*-value = 0.01).

3.2 Temporal Clustering Analysis

Most of the wild birds H5N1 outbreak peaks occurred during the winter period, which suggesting a character of seasonal cycle (figure 3).

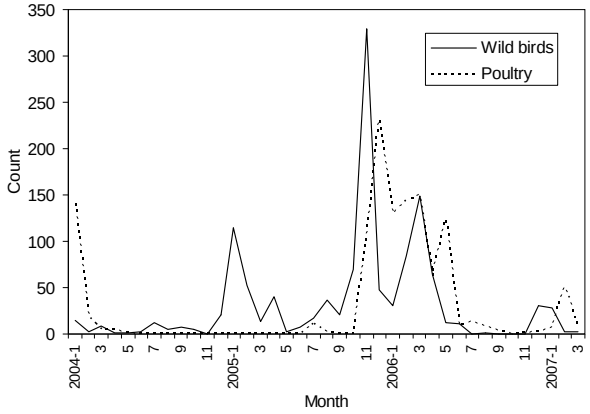

Figure. 3. The number of H5N1 outbreaks according to different species, wild birds and poultry

3.2.1 Autocorrelation Function: The autocorrelation function was found by using the residuals after fitting a linear model for lags from 0 to 48 months. The autocorrelation function (figure 4) is dominated by a 12-month periodicity. The time lags among the peaks (2 positive to positive, 1 negative to negative) are 14, 11 and 13 months apart.

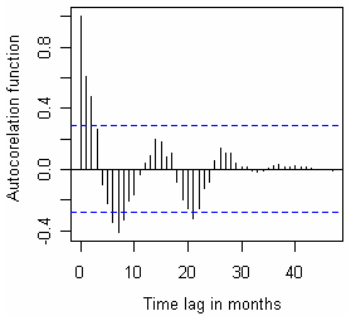

Figure. 4. The Autocorrelation function of the monthly time series of H5N1 outbreaks worldwide between December 2003 and December 2007, with 95% confidence limits.

3.2.2 Periodogram

The periodogram of the time period confirms the approximate 12-month period to the variability in the time series.

3.3 Space-time clustering analysis

3.3.1 Knox test: The result of Knox test in table 1 suggested the presence of significant space-time interaction $(p < 0.01)$ in all critical spatial (10 km and 4374 km) and temporal (21 and 320 days) thresholds.

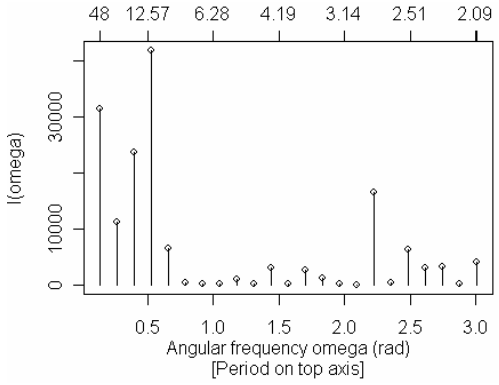

Figure. 5. Periodogram of the time series of monthly reported H5N1 outbreaks worldwide

Space (km)	Time (day)	Observed outbreaks	Expected outbreaks	*p*-value
10	21	2671	337	< 0.05
4374	320	1844023	1587416	< 0.05

Table 1: Results of the Knox test showing the number of observed and expected pairs of H5N1 disease worldwide from December 2003 to March 2007.

3.3.2 Space-time *K* Function: The $\hat{Do}(d,t)$ plot in figure 6 shows a large proportion of incident cases (risk) within 10 km and 21 days, and provides visual evidence of space-time clustering. The formal test of significance using 999 Monte Carlo simulations by generating a set of simulated summed *D* values, with only one exceeding the observed value (figure 6). These results imply that there is significant space-time clustering in the H5N1 outbreak data $(p < 0.001)$, supporting the hypothesis that H5N1 is the result of some infectious agent.

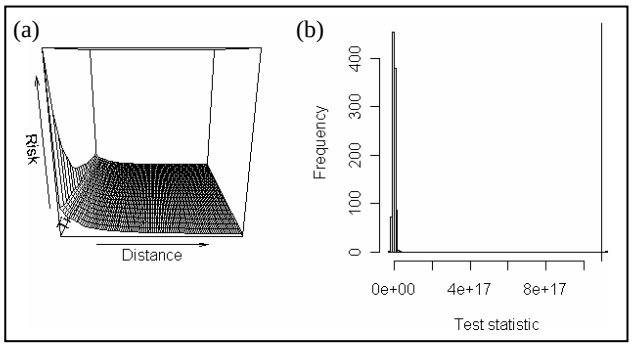

Figure. 6.(a) A 3-dimensional plot of the $\hat{Do}(d,t)$ function for H5N1 outbreaks, (b) testing H5N1 data for space-time interaction (b)

3.3.3 Space-time permutation scan statistics: One hundred and four significant space-time clusters $(p < 0.05)$ were detected by space-time permutation scan statistics (Figure 7). The black dots showed all H5N1 outbreaks worldwide between December 2003 and March 2007, while the red circles showed the location of the space-time clusters.

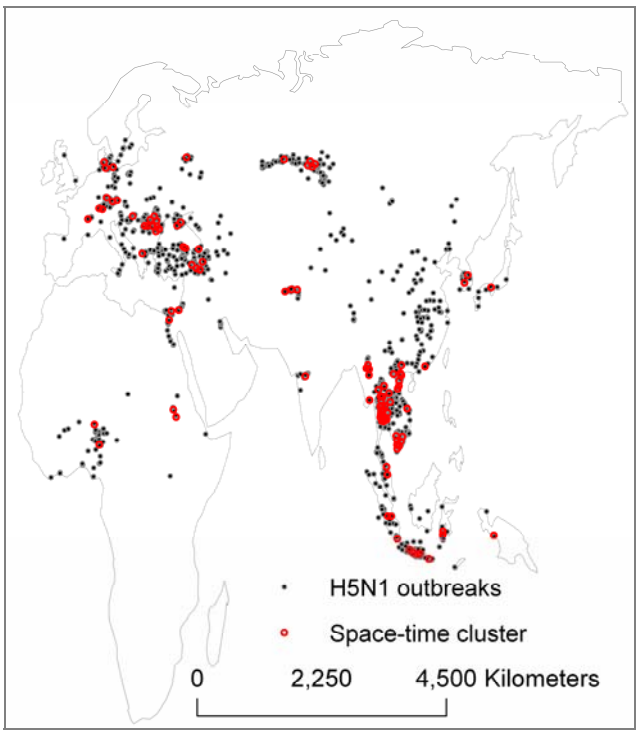

Figure. 7. Space-time clusters of H5N1 outbreaks detected by space-time permutation scan statistics.

4. DISCUSSION

This study has explored the spatial, temporal and space-time clustering of highly pathogenic H5N1 outbreak in 3-year period at the global scale. According to kernel estimation, the highest density areas are South Asia, East Russia, West Europe, Black Sea, and East Africa. The results of *G* and *F* functions showed that the disease outbreak is clustering significantly in the geographical scale. The outbreak of H5N1 also had a character of seasonality, and most of the cases are reported during the winter period. The autocorrelation function and periodogram showed the cyclical time is about 12 months. The significant space-time clustering was tested by both Knox's test and space-time K function. In terms of disease hot spots, space-time permutation scan statistics detected one hundred and four space-time clusters which are widely distributed in South Asia, East Russia, West Europe, Black Sea, and East Africa. These areas are suggested to be a high risk area for which warning systems should be targeted at.

These analyses are based on the online reported cases. The data source is inevitably bias. Some cases would be reported late or ignored because of the medical treatment level and government publicity. However, this is the most reliable data source we could obtain at present; the analyzing results can shed some light on spatial and temporal patterns of the highly pathogenic H5N1 outbreak both at the global and regional scales.

For the temporal pattern analysis, the disease showed a preference to cool temperatures. However, the outbreak period is not exactly 12 months. That is possibly because most of the countries in South Asia and Africa have no big temperature difference between summer and winter, which may influence the detection of outbreak seasonality.

The future work will focus on the possibly spreading directions of highly pathogenic H5N1 both at the global and regional scales. This will furthermore provide valuable information in understanding the global spread of H5N1 and surveillance.

5. CONCLUSIONS

This study resulted in the following conclusions:

- The disease outbreak of H5N1 clusters significantly in the spatial scale. The highest density areas are South Asia, East Russia, West Europe, Black Sea, and East Africa.
- The outbreak of H5N1 showed a temporal clustering in winter period with a 12-month cycle.
- Significant space-time clustering occurred in global H5N1 outbreaks. The locations of one hundred and four space-time clusters are suggested to be hot spot areas.

ACKNOWLEGEMENTS

This research is sponsored by the China Scholarship Council and the International Institute for Geo-Information Science and Earth Observation (ITC). We thank Dr. Willem Nieuwenhuis for his help in programming.

REFERENCE

Assuncao, R., Tavares, A., Correa, T. and Kulldorff, M., 2007. Space-time cluster identification in point processes. The Canadian Journal of Statistics, 35(1), pp. 9-25.

Bailey, T. C. and Gatrell, A. C., 1995. Interactive spatial data analysis. Longman Scientific & Technical, England, pp. 413.

Diggle, P. J., 1990. Time Series: A Biostatistical Introduction. Oxford University Press Oxford, pp. 257.

Diggle, P. J., Chetwynd, A. G., Haggkvist, R. and Morris, S. E., 1995. Second-order analysis of space-time clustering. Statistical Methods In Medical Research, 4, pp. 124-136.

French, N. P., Berriatua, E., Wall, R., Smithb, K. and Morgan, K. L., 1999. Sheep scab outbreaks in Great Britain between 1973 and 1992: spatial and temporal patterns. Veterinary Parasitology, 83(3-4), pp. 187-200.

French, N. P., Mccarthy, H. E., Diggle, P. J. and Proudman, C. J., 2005. Clustering of equine grass sickness cases in the United Kingdom: a study considering the effect of position-dependent reporting on the space-time K-function. Epidemiology and Infection, 133, pp. 343-348.

Gatrell, A. C., Bailey, T. C., Diggle, P. J. and Rowlingson, B. S., 1996. Spatial Point Pattern Analysis and Its Application in Geographical Epidemiology. Transactions of the Institute of British Geographers, 21(1), pp. 256-274.

Knox, E. G. and Bartlett, M. S., 1964. The Detection of Space-Time Interactions. Applied Statistics, 13(1), pp. 25-30.

Kulldorff, M., 1997. A Spatial Scan Statistic. Communications in Statistics - Theory and Method, 26(6), pp. 1481-1496.

Kulldorff, M., 2006. SaTScan User Guide. http://www.satscan.org/

Kulldorff, M., Heffernan, R., Hartman, J., Assuncao, R. and Mostashari, F., 2005. A Space -Time Permutation Scan Statistic for Disease Outbreak Detection. PLoS Medicine, 2(3), pp. 216-224.

Kulldorff, M. and Hjalmars, U., 1999. The Knox Method and Other Tests for Space-Time Interaction. Biometrics, 55(2), pp. 544-552.

Mcnally, R. J. Q., Alexander, F. E. and Bithell, J. F., 2006. Space-time clustering of childhood cancer in Great Britain: A national study, 1969-1993. International Journal of Cancer, 118, pp. 2840-2846.

Mulatti, P., Kitron, U., Mannelli, A., Ferre, N. and Marangon, S., 2007. Spatijal Analysis of the 1999-2000 Highly Pathogenic Avian Influenza (H7N1) Epidemic in Northern Italy. Avian Diseases, 51, pp. 421-424.

Norstrom, M., Pfeiffer, D. U. and Jarp, J., 2000. A space-time cluster investigation of an outbreak of acute respiratory disease in Norwegian cattle herds. Preventive Veterinary Medicine, 47, pp. 107-119.

Oie, 2006. DISEASE INFORMATION 2 February 2006; Vol. 19 - No. 5. http://www.oie.int/eng/info/hebdo/AIS_33.HTM

Oyana, T. J., Dai, D. and Scott, K. E., 2006. Spatiotemporal Distributions of Reported Cases of the Avian Influenza H5N1 (Bird Flu) in Southern China in Early 2004. Avian Diseases, 50(4), pp. 508-515.

Picado, A., Guitian, F. J. and Pfeiffer, D. U., 2007. Space–time interaction as an indicator of local spread during the 2001 FMD outbreak in the UK. Preventive Veterinary Medicine, 79, pp. 3-19.

Rogerson, P. A., 2001. Monitoring Point Patterns for the Development of Space-Time Clusters. Journal of the Royal Statistical Society, 164(1), pp. 87-96.

Walter, C., Mcbratney, A. B., Rossel, R. A. V. and Markus, J. A., 2005. Spatial point-process statistics: concepts and application to the analysis of lead contamination in urban soil. Environmetrics, 16, pp. 339-355.

Ward, M. P., Maftei, D., Apostu, C. and Suru, A., 2008. Geostatistical visualisation and spatial statistics for evaluation of the dispersion of epidemic highly pathogenic avian influenza subtype H5N1. Veterinary Research, 39(3).

Who, 2004. Avian Influenza A (H5N1) in Humans and Poultry in Viet Nam. http://www.who.int/csr/don/2004_01_13/en/

Who, 2007. H5N1 avian influenza: Timeline of major events. http://www.who.int/csr/disease/avian_influenza/ai_timeline/en/index.html

Wilesmith, J. W., Stevenson, M. A., King, C. B. and Morris, R. S., 2003. Spatio-temporal epidemiology of foot-and-mouth disease in two counties of Great Britain in 2001. Preventive Veterinary Medicine 61(3), pp. 157-170.